Science of the Total Environment 838 (2022) 156543

Contents lists available at ScienceDirect

Science of the Total Environment

journal homepage: www.elsevier.com/locate/scitotenv

Black carbon toxicity dependence on particle coating: Measurements with a novel cell exposure method

Henri Hakkarainen [a,*], Laura Salo [b], Santtu Mikkonen [c,d], Sanna Saarikoski [e], Minna Aurela [e], Kimmo Teinilä [e], Mika Ihalainen [a], Sampsa Martikainen [b], Petteri Marjanen [b], Teemu Lepistö [b], Niina Kuittinen [b], Karri Saarnio [e], Päivi Aakko-Saksa [f], Tobias V. Pfeiffer [g], Hilkka Timonen [e], Topi Rönkkö [b], Pasi I. Jalava [a]

[a] Inhalation Toxicology Laboratory, Department of Environmental and Biological Sciences, University of Eastern Finland, P.O. Box 1627, 70211 Kuopio, Finland
[b] Aerosol Physics Laboratory, Physics Unit, Tampere University, P.O. Box 692, 33014 Tampere, Finland
[c] Department of Applied Physics, University of Eastern Finland, P.O. Box 1627, 70211 Kuopio, Finland
[d] Department of Environmental and Biological Sciences, University of Eastern Finland, P.O. Box 1627, 70211 Kuopio, Finland
[e] Atmospheric Composition Research, Finnish Meteorological Institute, P.O. Box 503, Helsinki 00101, Finland
[f] VTT Technical Research Centre of Finland, P.O. Box 1000, 02044 VTT Espoo, Finland
[g] VSParticle B.V., Molengraaffsingel 10, 2629 JD Delft, the Netherlands

HIGHLIGHTS

- Toxicity of the differently treated combustion generated BC was studied with novel thermophoresis-based ALI system.
- Results show that organic compounds and the aging of the particles were major driver of the toxicity.
- Analysis pinpointed the effect of particle size to the toxicity, with decrease in particle size, increasing the toxicity.

GRAPHICAL ABSTRACT

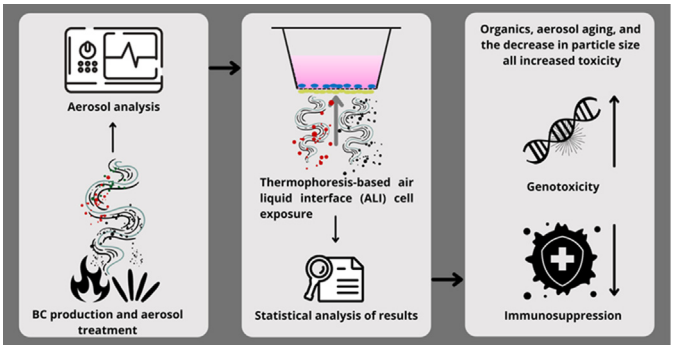

ARTICLE INFO

Editor: Lotfi Aleya

Keywords:
BC
PM
ALI
Genotoxicity
Inflammation

ABSTRACT

Black carbon (BC) is a component of ambient particulate matter which originates from incomplete combustion emissions. BC is regarded as an important short-lived climate forcer, and a significant public health hazard. These two concerns have made BC a focus in aerosol science. Even though, the toxicity of BC particles is well recognized, the mechanism of toxicity for BC as a part of the total gas and particle emission mixture from combustion is still largely unknown and studies concerning it are scarce. In the present study, using a novel thermophoresis-based air-liquid interface (ALI) *in vitro* exposure system, we studied the toxicity of combustion-generated aerosols containing high levels of BC, diluted to atmospheric levels (1 to 10 μg/m^3). Applying multiple different aerosol treatments, we simulated different sources and atmospheric aging processes, and utilizing several toxicological endpoints, we thoroughly examined emission toxicity. Our results revealed that an organic coating on the BC particles increased the toxicity, which was seen as larger genotoxicity and immunosuppression. Furthermore, aging of the aerosol also increased its toxicity. A deeper statistical analysis of the results supported our initial conclusions and additionally revealed that toxicity increased with decreasing particle size. These findings regarding BC toxicity can be applied to support policies and technologies to reduce the most hazardous compositions of BC emissions. Additionally, our study showed that the thermophoretic ALI system is both a suitable and useful tool for toxicological studies of emission aerosols.

* Corresponding author at: University of Eastern Finland, Department of Environmental and Biological Sciences, P. O. Box 1627, FI-70211 Kuopio, Finland.
E-mail address: Henri.hakkarainen@uef.fi (H. Hakkarainen).

http://dx.doi.org/10.1016/j.scitotenv.2022.156543
Received 11 February 2022; Received in revised form 3 June 2022; Accepted 3 June 2022
Available online 6 June 2022

1. Introduction

Air pollution is one of the main causes of premature deaths globally, with a death toll of up to seven million annually, and nine out of ten people's breathing levels of air pollution exceed the WHO guideline levels (WHO, 2021). Despite the vast evidence connecting air pollution with deaths and diseases, mortality due to outdoor pollution levels remains high (Ritchie and Roser, 2017). While the causality is clear, the relative importance of different chemical species found in ambient particles requires further research. Understanding distinct air pollution components and their role in human health is important (Cassee et al., 2013; Grahame et al., 2014; Adams et al., 2015). Besides particle chemistry, physical characteristics also influence toxicity. While the mass concentration of fine particles ($PM_{2.5}$) is the most measured metric, laboratory studies have found that particle surface area (SA) concentration better predicts toxicity (Schmid and Stoeger, 2016, Sager and Castranova, 2009). Overall, the chemistry and physical characteristics depend on the emission source, as well as atmospheric processes, further complicating the evaluation of particle toxicity for a certain emission source.

Black carbon (BC) particles originate from incomplete combustion in engines, residential heating and cooking, forest fires, power plant boilers, and other combustion processes. In urban areas, road traffic is generally the main source of BC, with some contributions from other sources, depending on the location (Saarikoski et al., 2021). Due to the relatively short atmospheric life of BC particles, their concentrations vary spatiotemporally from low, below 1 $\mu g/m^3$ (Hara et al., 2019; Vodička et al., 2020; Luoma et al., 2021) to very high, up to 10–20 $\mu g/m^3$ (Gramsch et al., 2020; Cai et al., 2020). Overall, the development of better exhaust after-treatment systems for vehicles, such as particulate filters, have led to the reduction of traffic emissions and declining of urban BC concentrations (Wihersaari et al., 2020; Luoma et al., 2021). Insoluble in water, BC particles are an efficient solar radiation absorber. Hence, BC is a prominent contributor to global climate change, particularly within the Arctic (Bond et al., 2013; Sand et al., 2016). BC particles consist of a carbon core comprising mainly elemental carbon (EC) and a surface that can act as a condensation area for toxic vapours released alongside BC (Ristimäki et al., 2007). The structures of fresh BC particles are fractal but would become compact after atmospheric aging (Kahnert, 2017).

In addition to climatic effects, BC particles are linked to several health effects (WHO, 2021). Some reviews of epidemiological studies have even suggested that BC particles are one of the most hazardous components of ambient aerosol (EPA, 2012; Janssen et al., 2012). However, other interpretations of current data have concluded that BC is only a small component contributing to $PM_{2.5}$ toxicity (Stanek et al., 2011) or that evidence either way is insufficient (Kirrane et al., 2019). Different physicochemical and morphological properties of particulate matter (PM) as well as simultaneously emitted species, co-emitted species, affect the toxicity of particles and subsequent health effects (Rönkkö et al., 2020). Similarly, BC particle toxicity can also be affected by particle size, morphology, and co-emitted species (Wang et al., 2019), as well as by atmospheric aging impacted by several environmental parameters. BC can also work as carrier for different toxic compounds, for example, multiple different organic components (Cassee et al., 2013). Therefore, to simulate real-life conditions, studying BC toxicity with various surface coatings is crucial. Overall, the importance of BC as a research focus is indisputable, as mitigation of BC emissions would result in major benefits for both climate change and air quality (Timonen et al., 2019).

To date, toxicological studies concerning BC have mostly used carbon black (CB) as a substitute for combustion-originated BC. Considering how difficult the process of separating BC from a PM mixture is, CB is easier to use in *in vitro* studies using submerged culture conditions. However, CB produced by industrial processes has a higher EC contribution (> 90 %) compared to BC and the particle surface of CB is more homogenous, which affects its ability to absorb components (Müller et al., 2007). Furthermore, unlike combustion, the CB synthesis process involves no co-emittance of toxic vapours. Due to these differences, CB should not be used as a BC substitute in toxicological studies (Long et al., 2013). To examine BC toxicity, exposure systems should aim to mimic real-life lungs and use BC created by combustion emissions. Such systems include the air-liquid interface (ALI), different organ-on-a-chip devices, and complicated multicellular culture systems. Besides conducting toxicology measurements, aerosol properties need to be measured simultaneously to account for changes in concentration, chemical composition, and particle size.

In the present study, using a thermophoresis-based ALI exposure system (Ihalainen et al., 2019), we simultaneously exposed two cell lines mimicking the lung alveolar region to combustion-generated aerosol containing atmospheric levels of BC. The two cell lines were the human adenocarcinomic alveolar epithelial cell line (A549) and human monocytic leukemia cell line (THP-1) co-culture. Applying multiple different aerosol treatments, we simulated different sources and atmospheric aging processes. Utilizing several toxicological endpoints, we could thoroughly examine emission toxicity. Overall, our results contribute valuable data on toxicological effects connected to combustion-generated BC.

2. Materials and methods

2.1. Generation of the aerosols

The particle generation was designed to produce BC particles representing different phases of BC's lifetime, *i.e.*, primary BC particles (later called as Primary), BC particles accompanied by sulfuric acid and hydrocarbons that exist in fresh exhaust (later Fresh), and aged BC containing aerosol (later called as Aged). This was done by generating BC by burning propane in a flat flame type gas burner (GB) (Holthuis & Associates), equipped with mass-flow controlled fuel, oxygen, and nitrogen supplies, by mixing hydrocarbons (octacosane in case of Fresh and benzene in case of Aged) and sulfuric acid with BC, and by using appropriate dilution and cooling system to mimic particles of fresh exhaust and aging chamber to produce the aged BC containing aerosol. In addition to six different aerosols generated by this setup, two test points were also conducted with BC particles produced by spark generator (model VSP-G1, by VSParticle, (Boeije et al., 2020)), with solid carbon electrodes and N_2. Because the particles are ablated in an inert atmosphere, no combustion side-products are expected. See Table 1 for the details of different aerosol exposures. Fig. 1 shows a simplified diagram of the setup, while a detailed one is included in the supplementary material (Supplementary materials S1 Fig. 1). Hydrocarbons were added prior to dilution, with the sample kept at a hot temperature (~300 °C). The sulfuric acid was generated by feeding sulfur dioxide into the sample line prior to the dilution stages through an oxidative catalyst (Karjalainen et al., 2017).

The above-mentioned dilution and cooling system which mimics fresh exhaust dilution consisted of a combination of a porous tube diluter (PTD), residence time tube (RTT) and an ejector diluter (Fig. 1). This type of dilution mimics the dilution, cooling, relative humidity, and particle formation processes that happen when the exhaust aerosol from a combustion engine exits the tailpipe and enters the atmosphere (Ntziachristos et al., 2004; Mathis et al., 2004; Keskinen and Rönkkö, 2010). It allows the transferring of initially gaseous, semi-volatile compounds to particulate phase. The dilution system has been previously used to characterize several the real-world particle emissions of vehicles and other combustion applications

Table 1
Test point descriptions. VSP-GI is a spark generator.

Test point	BC source	Aerosol treatment	Particle coating
Primary	Gas burner	Primary	–
Fresh	Gas burner	Fresh	–
$Fresh_{HC}$	Gas burner	Fresh	Octacosane
$Fresh_{H2SO4}$	Gas burner	Fresh	Sulfuric acid
$Aged_{1d}$	Gas burner	Aged, 1 day	Benzene (precursor)
$Aged_{5d}$	Gas burner	Aged, 5 days	Benzene (precursor)
$Fresh_{VSP}$	VSP-G1	Fresh	–
$Fresh_{VSP, HC}$	VSP-G1	Fresh	Octacosane

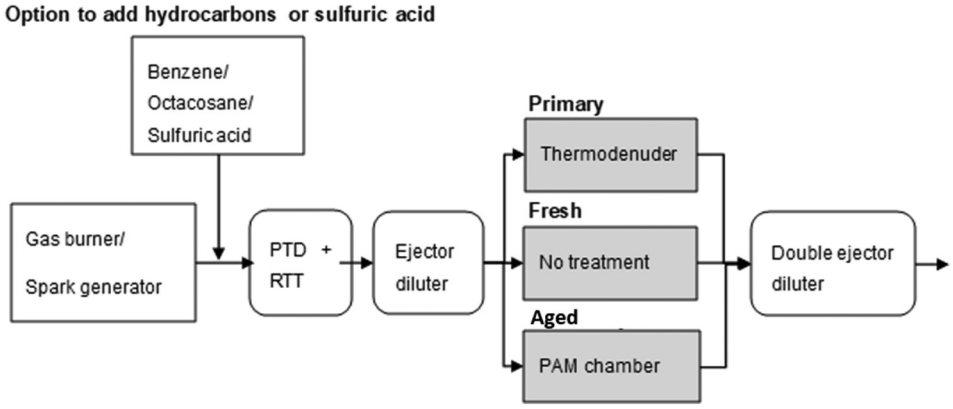

Fig. 1. Simplified diagram of the aerosol production setup. After the double ejector diluter, the aerosol is directed to ALI and other instrumentation. A detailed diagram is provided in the supplementary material (Supplementary Materials S1 Fig. 1).

(Rönkkö et al., 2007; Karjalainen et al., 2014). In this study, the total dilution rate (DR) of the system ranged from 600 to 1000 (lower during fresh or primary measurements and higher during aged aerosol measurements).

After these dilution stages, the sample was either left untreated (Fig. 1: Fresh), led through a thermodenuder (Fig. 1: Primary, Saha et al., 2015; Rönkkö et al., 2011; Heikkilä et al., 2009) or led through a PAM chamber (Fig. 1: Aged, Potential Aerosol Mass chamber, Kang et al., 2007, Timonen et al., 2017). With the Primary samples, the aerosol was led through a thermodenuder, in which the diluted exhaust sample is heated to 265 °C, which causes evaporation of the most volatile aerosol particles and condensated compounds. Evaporated compounds are then removed, leaving mainly the non-volatile particle cores in the sample. With the Aged samples, the PAM chamber mimics atmospheric aging by producing main atmospheric oxidants (O_3, OH-and HO_2-radicals), that can react with the existing precursor gases/vapours (*e.g.* benzene) in the chamber (Kang et al., 2007; Lambe et al., 2011). This oxidates the particles similarly as in the atmosphere, but significantly faster due to higher oxidant concentrations. However, in addition to increase in mass the aging of benzene may lead to photodegradation, which generate compounds with smaller molecular weight and high volatility (Borrás and Tortajada-Genaro, 2012). These samples correspond to the phases of engine-emitted aerosol, with Primary being the aerosol inside the tailpipe, Fresh the aerosol a few seconds after being released into the atmosphere and cooled to ambient temperatures and Aged the aerosol which forms over hours and days in the atmosphere. In the final dilution stage, two adjacent ejector diluters were used to increase the sample flow rate to have enough sample for all instruments.

Particle size distribution was measured with a scanning mobility particle sizer (SMPS, TSI; Wang and Flagan, 1990). Particle number (PN) was measured with a condensation particle counter for particles with a diameter larger than 10 nm (A20 CPC, Airmodus), and surface area of particles was determined from data measured with an electrical low-pressure impactor (ELPI+, Dekati Ltd.; Järvinen et al., 2014; Keskinen et al., 1992). BC concentration was measured using an aethalometer (AE33, Aerosol d.o.o., Ljubljana, Slovenia; Drinovec et al., 2015; Hansen et al., 1984) and other compounds of PM with a soot particle aerosol mass spectrometer (SP-AMS, Aerodyne Research Inc. Billerica, US; Onasch et al., 2012).

2.2. ALI exposure

The thermophoresis effect -based ALI system (Ihalainen et al., 2019) was used to assess cytokine release, DNA damage, and differences in cell cycle phases from the exposed cells. The thermophoresis-based ALI exposure is presented in the Fig. 2. The main flow in ALI was 5 l/min with relative humidity approaching 100 %, while still staying below the condensation point at 37 °C. A partial flow of 150 ml/min was led to the cell surfaces as a laminar flow. A total of three independent 1-h exposures ($n = 3$) were conducted for each test point, along with exposures of clean air, incubator, and positive controls. The clean air exposures ($n = 8$) were used as control for the different toxicological analyses. Incubator control (n = 8) was used as control for the ALI exposure system, and the positive controls (n = 8) were lipopolysaccharide (LPS) for cytokine and methyl methanesulfonate (MMS) for genotoxicity analyses.

2.3. Cell culture

Cell lines of A549 human alveolar epithelial cells (ATCC®, CCL-158™) and THP-1 human monocyte cells (DSMZ ACC 16; German Collection of Micro-organisms and Cell Cultures; DSMZ, Germany) were cultured in a humidified incubator at +37 °C and 5 % CO_2 in Dulbecco's Modified Eagle (DMEM) supplemented with 10 % (*v*/v) fetal bovine serum (FBS), 2 mM L-glutamine, and 100 U/ml penicillin/streptomycin (Sigma-Aldrich or Gibco, Life technologies). Co-culture of A549 and THP-1 cells were cultured on 24 mm Falcon™ inserts (Corning, #353090, USA), the A549 cells resemble the lung alveolar epithelial cells and addition of THP-1 simulates macrophages within the lungs, thus, resulting in a cell model which aims to mimic the lung alveolar area. The A549 cells were cultured on the basal side of the inserts' membrane for four to six days prior to exposures. Seeding density of the cells depended on the exposure day and were the following: 220 000 cells/ml for inserts exposed four days later, 200 000 cells/ml for inserts exposed five days later, and 180 000 cells/ml for inserts six days later. Inserts were kept on 6-well plates with a total of 1 ml of 10 % FBS DMEM on both sides of inserts. Two days (48 h) prior to exposure, the ALI environment was formed for A549 cells by removing the cell medium and adding 1 ml of DMEM with 5 % of FBS only onto the apical side. One day (24 h) prior to exposure, THP-1 cells differentiated with 0.5 μg ml^{-1} phorbol-12-myristate-13-acetate (PMA) were seeded onto the apical side of the inserts with the seeding density of 110 000 cells/ml, thus the amount of THP-1 s was approximately 10 % of the total cell count during the exposure. Immediately before the exposure, the medium on the apical side was replaced with a serum free medium with a 25 mM 4-(2-hydroxyethyl)-1-piperazineethanesulfonic acid (HEPES) buffer (Sigma-Aldrich, USA). HEPES resists pH changes during the exposure. After the one-hour exposure, the cell medium was collected for further analysis, a new medium with 0 % FBS was added, and cells were incubated for 24 h at +37 °C with 5 % CO_2.

After the 24 h incubation, the cell medium was again collected for the analysis, therefore, giving us a chance to analyse the cytokine levels both immediately (marked as 1 h) and 24 h after the exposure with enzyme-linked immunosorbent assay (ELISA). Following the cell medium collection, both sides of the inserts were washed with phosphate-buffered saline (PBS). The PBS was then collected into separate tubes and trypsin-ethylenediaminetetraacetic acid (EDTA) was added on the cells to detach the cells from the inserts' membranes. Trypsin-EDTA was allowed to affect

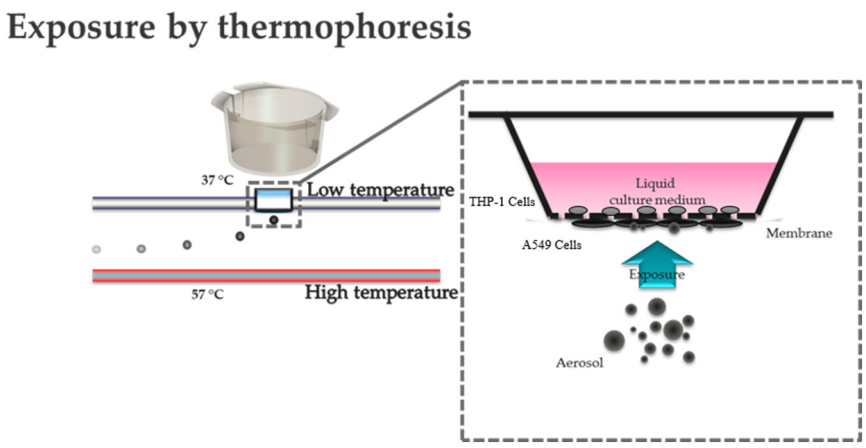

Fig. 2. Simplified presentation of the thermophoresis-based air liquid interface exposure inside the ALI system used in present study. Original picture by Mika Ihalainen, modified to display the A549 and THP-1 co-culture by the corresponding author.

the cells for 5 min at +37 °C with 5 % CO_2. After the trypsin-EDTA treatment, 100 μl of FBS was added to inhibit trypsin-EDTA action. Cells were rinsed from the insert membranes and collected into same tubes as the PBS. A portion of the collected cells were pipetted in droplets to 4 ml of 70 % (*v*/v) ethanol under constant vortexing and stored at +4 °C. These cells were later analysed with FACSCanto II flow cytometer (BD Biosciences, USA) to determine the cell cycle phase. Of the remaining cells, 60 μl were mixed with freezing medium (50 % DMEM, 40 % FBS and 10 % DMSO) and stored at −80 °C for later analysis of genotoxicity.

2.4. ALI deposition

Deposition of particle mass, number, and surface area can be estimated from the measured aerosol concentrations. These calculations are presented in supplementary materials S1.1 and results in Table 5. For this ALI system, the thermophoresis is the main deposition mechanism in contrast to diffusion- and sedimentation-based ALI systems (Ihalainen et al., 2019). Further information on how the deposition is calculated can be found in Ihantola et al. (2020).

2.5. Toxicological analyses

2.5.1. Genotoxicity

Genotoxicity was assessed with the slightly modified alkaline version of single-cell gel electrophoresis (SCGE), also known as the comet assay. In the SCGE assay, the cells are embedded in agarose gel and lysed in alkaline conditions, followed by electrophoresis. The lysing reveals the cell nucleoids, and the DNA supercoils, and the alkaline conditions relax the DNA coils, making the analysis of genotoxicity more robust. During the electrophoresis step, DNA strand breaks allow the negatively charged DNA to move towards the positive anode of the electrophoresis chamber. The migrated DNA-strands can be stained with ethidium bromide and quantified with fluorescence microscopy. The level of genotoxicity is therefore the ratio of migrated DNA compared to the unmigrated.

A 60 μl aliquot of cells was collected into Eppendorf-tubes with 540 μl of freezing medium (DMEM supplemented with 40 % (*v*/v) filtered FBS (BioWest, France) and 10 % (v/v) DMSO) and stored at −80 °C. For the SGCE-assay, the cell samples in the Eppendorf-tubes were partially thawed in a + 37 °C water bath and centrifuged for four minutes at +4 °C. After the centrifugation, most of the supernatant was removed. Cells were resuspended to remaining supernatant and from each tube, duplicates of 20 μl cell suspension aliquots were mixed in 80 μl of low melting point agarose (LMPA, 0.5 % in PBS) and 80 μl of the mixture was added on top of the normal melting point agarose (1 % PBS) coated microscope slides. This was followed by the lysis of cells by submerging slides into a lysis buffer (2.5 M NaCl, 100 mM disodium ethyl-enediaminetetraacetic acid (Na_2EDTA), 10 mM Trizma base, 200 mM NaOH, 1 % (*v*/v) Triton X-100 in ddH_20, pH 10) at +4 °C for one hour. After the lysis, slides were rinsed with the neutralizing buffer (0.4 M Tris(hydroxymethyl)aminomethane, pH 7.5) and carefully arranged in the electrophoresis tank. The tank was filled with a cold electrophoresis buffer (0.3 N NaOH, 1 mM Na2-EDTA, pH > 13), incubated for 40 min in the dark and followed by electrophoresis at to 24 V/300 mA for 20 min. After electrophoresis, the slides were neutralized by rinsing them three times with a neutralizing buffer, then fixed with ethanol (99 % v/v) and left to dry. After the drying, the slides were stained with ethidium bromide, which binds between DNA bases and emits fluorescence under fluorescent light, and a total of 100 cells from the duplicate slides per sample were scored with a fluorescence microscope Zeiss Axio Observer Z1 (ZEISS, Germany) using Comet assay IV software (Perspective Instruments Ltd., UK). Data analysis and statistical analysis was done using the median from the percentage of DNA in the tail, since it has been proven to yield results that are easier to compare between different studies (Sunjog et al., 2013).

2.5.2. Cytokines

The inflammatory response of the cells was analysed by measuring the concentration of cytokines CXCL8/IL8, CXCL1/Gro-a, and TNF-α. The selection of inflammatory mediators was based on results from previous studies (Ihantola et al., 2020; Ihantola et al., 2022). The cytokines were measured from the cell culture medium collected immediately after the exposures and after 24-h incubation, using ELISA kit (R&D Systems, Abington, UK) on 96-well plates (Nunc Maxisorp), according to the manufacturer's instructions. The measurements were conducted with hybrid multi-mode reader Synergy H1 (BioTek Instruments, USA) at 450 nm. The concentrations of cytokines were interpolated from the standard curves.

2.5.3. Cell cycle

In a cell cycle assay, the RNA of the fixed and permeabilized cells is first removed, followed by the staining of the DNA with propidium iodide (PI), a fluorescent agent which binds to the DNA through intercalation between the bases. The stained DNA inside cells produce fluorescence signals proportional to the amount of cellular DNA. Because PI binds to RNA as well, the fluorescence signal from RNA would make the results impossible to interpret, which is why the RNA is removed.

The cell suspensions fixed with ethanol were centrifuged, washed with 1 ml of cold PBS, and resuspended in 250 μl of cold PBS. After this, 3.75 μl of RNAse A (10 mg/ml) was added to the samples and the samples were vortexed prior to a 1-h incubation at +50 °C, followed by an addition of 2.0 μl of PI (1 mg/ml) to the samples, vortexing and a 30 min incubation at +37 °C. The samples were measured with a FACSCanto II flow cytometer (BD Biosciences, USA). The data from the measurements was analysed

using FlowJo 10 software (FlowJo LLC, USA) and presented as cell population percentages in sub-G1/G0, G1/G0, and S + G2/M phases.

2.6. Statistical methods

The Multivariate Mixed Model (MMM, Mehtätalo and Lappi, 2020) was used to assess how the aerosol particle concentration and select individual chemical components contributed to the observed toxicological responses. The main idea of a mixed model is to estimate not only the mean of the measured response variable but also the variance-covariance structure of the data. This makes the model applicable also for atmospheric measurement data, which do not usually fulfill the standard independency and homogeneity assumptions required by most regression or ANOVA type statistical models (Mikkonen et al., 2011). Additionally, modelling the covariance structure of the variables makes the estimates more accurate and prevents autocorrelation of the residuals. The model is formed by adding a so-called random component to the standard linear model, in matrix format given by $y = \beta X + \varepsilon$, where y is the vector of measurements of the studied variable, X is the matrix of observations from predictor variables, β denotes the unknown vector of intercept and slope estimates of the model and ε contains the residuals of the model. In the random part (denoted Zu), Z is the design matrix for the vector of random covariates u. Thus, the final models are given in form $y = \beta X + Zu + \varepsilon$. Experiment type and number of the sample were assigned as random effects due to the non-independence of chemical composition within each level of these factors.

The best predictive models for each toxicological endpoint in the MMM was achieved by testing all possible two predictor models and selecting three predictor models and comparing the changes in the Schwarz's Bayesian Criterion (BIC) value. Larger changes in BIC indicate larger explanatory power of the removed principal component (PC) on the dependent variable, *i.e.*, toxicological endpoint. Models with more than three predictors were not possible to fit as the number of observations did not allow it. MMM analyses were conducted for multiple different toxicological endpoints in both GB and VSP-G1 exposures, using several combinations of different aerosols parameters.

Statistical analyses were performed using IBM SPSS Statistics for Windows, Version 27.0 (IBM Corp. Armonk, NY) and R software (R Core Team, 2021; Bates et al., 2015).

3. Results

3.1. Aerosol properties

Table 2 shows the composition of the measured aerosol mass concentration. These results are used to interpret the cell culture data. Despite the efforts to keep the mass concentration, and especially BC concentration, consistent between points, there was variation. The total mass concentration (sum of analysed particulate components) ranged from 1.53 to 9.50 μg/m^3, while the BC concentration ranged from 1.22 μg/m^3 to 8.35 μg/m^3. The PM consisted mainly of BC and organic matter, here on referred as organic aerosol (OA), with small amounts of sulphate (SO_4^{2-}), which was present with the highest amount, when sulfuric acid was added to the test point $Fresh_{H2SO4}$. The contribution of the OA to the PM was highest when octacosane or benzene were added. OA:BC varied from 0.10 (Primary) to 3.90 ($Aged_{5d}$) indicating the thickness of the coating compared to the BC core. The percentage of organic aerosol when octacosane was added is somewhere between pure engine exhaust (Kostenidou et al., 2021) and traffic site ambient aerosol (Enroth et al., 2016).

Table 3
Mean mass concentrations of the different OA families during each test exposures. Oxidation state for OA was calculated as 2*(oxygen-to-carbon ratio) – (hydrogen-to-carbon ratio).

Test point	C_xH_y (μg/m^3)	C_xH_yO (μg/m^3)	$C_xH_yO_z$ (z > 1) (μg/m^3)	C_xH_yN (μg/m^3)	Oxidation state
Primary	0.24	0.05	0.30	0.01	0.82
Fresh	0.09	0.03	0.07	0.01	−0.27
$Fresh_{HC}$	1.77	0.06	0.18	0.02	−1.80
$Fresh_{H2SO4}$	0.35	0.05	0.23	0.02	−0.07
$Aged_{1d}$	0.35	0.29	0.34	0.02	0.43
$Aged_{5d}$	1.24	2.47	2.37	0.06	1.37
$Fresh_{VSP}$	0.09	0.03	0.08	0.02	−0.42
$Fresh_{VSP,\ HC}$	0.32	0.04	0.08	0.03	−1.41

The OA was further divided to different organic families based on the elemental composition (Table 3). In every test point, a large fraction of OA was composed of hydrocarbon fragments (C_xH_y), for which the largest fraction was measured for the test $Fresh_{HC}$ (87 % of the OA was C_xH_y) and smallest for test named $Aged_{5d}$ (20 % of the OA was C_xH_y). The OA in both $Aged_{1d}$ and $Aged_{5d}$ samples was constituted mostly of oxygenated fragments with one oxygen atom (C_xH_yO) or more than one oxygen ($C_xH_yO_z$ (z > 1)), the total fraction of oxygenated fragments being 63 % and 79 % in $Aged_{1d}$ and $Aged_{5d}$ samples, respectively. In terms of oxidation state of OA, $Aged_{5d}$ had clearly larger oxidation state than $Aged_{1d}$, whereas $Fresh_{HC}$ and $Fresh_{VSP,\ HC}$ had the smallest oxidation states for OA of all test points. The contribution of nitrogen-containing organic fragments (C_xH_yN) was 1–6 % in the OA. The largest fraction of it was measured for test $Fresh_{VSP,\ HC}$, however, the concentration of the total OA was rather small in this test point, and therefore, the inaccuracy in the C_xH_yN fraction was considerable.

Table 4 contains the particle number concentration, the particle surface area concentration, and the median particle aerodynamic size for the surface area distribution (SMAD: surface median aerodynamic diameter). The PN concentration varied among the test points even more than the mass concentration, but this was mostly due to the presence of nucleation mode particles in some test points. The particle number distributions of test points $Fresh_{H2SO4}$ to $Aged_{5d}$ and $Fresh_{VSP,\ HC}$ were bimodally distributed (see Supplementary materials S1 Fig. 2). In the aged aerosol cases there were so many nucleation mode particles that the soot mode was obscured. Table 4 also shows the particle SA concentration, which varied from 70 to 1440 μm^2/cm^3, and the median particle size of the SA distribution, which ranged from 43 to 281 nm. We chose the median of the SA distribution to represent the overall size, as especially in the case of the aged aerosols, the median of the number distribution was heavily influenced

Table 2
Mean mass concentrations of the different components and percent of organic aerosols (OA) from aerosols of each exposure. BC was measured with an aethalometer and other particulate components with the SP-AMS. Concentrations of carbon monoxide and ozone for each test point were measured with electrochemical gas sensors provided by Vaisala. Test points 5 and 6 contained addition of benzene in the PAM chamber. HC means addition of octacosane.

Test point	Total mass (μg/m^3)	BC (μg/m^3)	OA (μg/m^3)	SO_4^{2-} (μg/m^3)	NO_3^- (ng/m^3)	NH_4^+ (ng/m^3)	CO (ppm)	O_3 (ppm)	OA (%)
Primary	8.79	7.97	0.79	0.01	370	290	< 0.1	< 0.1	9.0
Fresh	1.53	1.22	0.30	0.01	680	620	< 0.1	< 0.1	19.6
$Fresh_{HC}$	6.28	4.09	2.15	0.01	500	570	< 0.1	< 0.1	34.3
$Fresh_{H2SO4}$	9.43	8.35	0.90	0.17	560	0.00	< 0.1	< 0.1	9.6
$Aged_{1d}$	5.30	3.98	1.29	0.02	760	180	2.92	0.45	24.3
$Aged_{5d}$	9.50	1.91	7.45	0.10	760	440	2.82	3.42	78.4
$Fresh_{VSP}$	1.61	1.30	0.28	0.01	320	370	< 0.1	< 0.1	17.5
$Fresh_{VSP,\ HC}$	1.93	1.40	0.53	0.01	300	0.00	< 0.1	< 0.1	27.5

Table 4
Particle number concentration measured with a CPC, particle surface area (SA) concentration measured with an ELPI+ and median of particle SA distribution for the surface area distribution. For the aged aerosol samples the soot mode could not be distinguished from the nucleation mode.

Test point	Particle number concentration (1/cm^3)	SA concentration (μm^2/cm^3)	Median of SA distribution (nm)
Primary	760	260	262
Fresh	1950[a]	70	72
$Fresh_{HC}$	270	130	276
$Fresh_{H2SO4}$	890	210	281
$Aged_{1d}$	74,800	390	86
$Aged_{5d}$	221,000	1440	78
$Fresh_{VSP}$	16,800	160[b]	24
$Fresh_{VSP, HC}$	11,700	110[b]	43

[a] CPC data for this measurement was not recorded, used SMPS measurement instead (1 out of 3 total hours recorded).
[b] Data partially recorded (2 h of 3 total hours).

by the nucleation mode particles. The spark generator soot particles were considerably smaller than the gas burner soot particles.

The primary BC particle distribution was not entirely consistent between test points, and especially for Fresh the primary distribution had a smaller median size than other test points, as can be seen Supplementary S1 Fig. 4, which shows the primary aerosol distribution for each one. The thermodenuder also has lower penetration for small particles, which leads to the Primary aerosol slightly shifting to a larger median size than the "true" Primary aerosol created in the flame.

Table 5 shows the deposition estimates within the thermophoresis-based ALI system.

3.2. Toxicological results

The toxicological results are presented in more detail in supplementary materials S1 Tables 1 and 2.

3.2.1. Genotoxicity

Genotoxicity results from Comet assay are presented in Fig. 3, with the mean of the three one-hour exposures compared to the clean air control and error bars showing the standard error of mean (SEM). With exception of Primary, all the aerosol exposures resulted in more genotoxicity than the control. The highest genotoxicity was observed from the $Aged_{5d}$ and $Fresh_{VSP}$ exposures.

3.2.2. Cytokines

Results of CXCL1 and IL8 measurements are presented in Figs. 4 and 5, respectively. The 1 h levels of CXCL1 were higher than the 24 h levels in all cases, and higher than the control level in all but $Aged_{5d}$. Clearly, the highest level from 1 h samples were detected from exposure to $Fresh_{HC}$, but in 24 h the levels of CXCL1 diminished below the levels of the clean air control sample. The highest 24 h level were detected from exposure of Primary and the lowest, for both 1 h and 24 h, from $Aged_{5d}$. For the IL8, a similar trend was observed, with 1 h levels being higher than 24 h levels. However, the highest 1 h levels for IL8 was detected from $Fresh_{VSP}$ and the lowest from $Aged_{5d}$. For the 24 h levels, the highest were seen from exposure to Primary and the lowest from the three coated ones, $Fresh_{H2SO4}$, $Fresh_{HC}$, and $Aged_{5d}$, which were all in the same range.

Table 5
Deposition estimates with SD for BC, PM (particulate matter), PN (particulate number) and SA (surface area) within the ALI system.

Test point	BC (ng/cm^2)	PM (ng/cm^2)	PN (#/mm^2)	SA (μm^2/mm^2)
Primary	0.72 ± 0.09	0.8 ± 0.11	730 ± 256	236 ± 57
Fresh	0.11 ± 0.01	0.14 ± 0.01	580 ± 826	65 ± 1
$Fresh_{HC}$	0.38 ± 0.11	0.58 ± 0.14	270 ± 124	121 ± 34
$Fresh_{H2SO4}$	0.76 ± 0.10	0.86 ± 0.11	1040 ± 771	192 ± 50
$Aged_{1d}$	0.36 ± 0.02	0.48 ± 0.04	67,300 ± 3185	353 ± 35
$Aged_{5d}$	0.18 ± 0.04	0.86 ± 0.12	199,000 ± 5683	1297 ± 20
$Fresh_{VSP}$	0.12 ± 0.03	0.15 ± 0.02	15,400 ± 3146	140 ± 29
$Fresh_{VSP, HC}$	0.13 ± 0.02	0.18 ± 0.03	14,000 ± 10,122	95 ± 10

3.2.3. Cell cycle

Different cell cycle phases analysed with flowcytometry are presented in Fig. 6. Exposures to Primary, $Fresh_{H2SO4}$, and, $Aged_{5d}$ resulted in notably different cell cycle phase fractions compared to the clean air control, with a higher amount of G1 phase for exposures of Primary and $Fresh_{H2SO4}$, and close to double amount of Sub_G1 for $Aged_{5d}$ exposure. Note that for the $Aged_{5d}$, the sum of the cell cycle phases is below the 100 %, due to incapability to get data from some of the $Aged_{5d}$ samples.

3.3. Results from statistical analysis

Results are comprehensively displayed in the supplementary material S2 Tables 1–8. From these results, four combinations of aerosol properties were also chosen for display in Fig. 7 from the GB originating exposures. The combinations are total mass and organic mass, total mass and PN, total mass and SA, and total mass and median particle diameter of the SA distribution. These were chosen due to the biological importance and statistically significant differences. The error bars indicate the 95 % confidence interval (CI: 95 %). To visualise the differences between the aerosol components, compared to total particle mass in more detail, we calculated the MMM analysis for PN, SA, and particle diameter with unit values of 10,000 #/cm^3, 10 μm/cm^3, and 10 nm, for 24 h GB exposures. For VSP-G1 originating samples similar graphs were not completed, as within those samples the variance within the results was considerably large.

4. Discussion

The present study demonstrates that *in vitro* exposures of combustion originated BC are possible with the novel thermophoresis-based ALI system, and that the different treatments of aerosol affect the observed toxicity. The statistical analyses uncovered the relationships between the aerosol properties and the toxicological results. As most of the previous studies concerning BC toxicity have used CB, instead of BC, the discussion was extended to include non-laboratory BC sources, such as diesel engines and wood burning. Overall, there is not yet a clear consensus on the toxicity of BC, as stated in the WHO global air quality guidelines 2021. Thus, the results of our study will contribute to future evaluations.

The difference in genotoxicity between the Primary and other GB originated samples indicate that the organic coating increases the DNA damage. The effect of organics to genotoxicity has been seen in previous studies, with compounds such as PAHs being the possible culprit (Billet et al., 2018; Kanashova et al., 2018; Ihantola et al., 2020; Ihantola et al., 2022). The PAH content may also vary highly due to different aerosol treatment, which might also explain the higher toxicity of Aged exposures. In cells such as A549 the genotoxicity of PAHs, especially the benzo[*a*]pyrene (B[*a*]P), is linked to the addition of metabolites to the amino groups of DNA, resulting in PAH DNA adducts, even with low concentrations of PAHs (Genies et al., 2013; Genies et al., 2016). However, in our study the concentrations of PAHs were not measured, thus, we can only speculate on their role. The results from the MMM analysis support the finding that organics increased genotoxicity, as the mass of organics in PM, as well as the addition of particle surface area, had a positive correlation with genotoxicity in the GB samples, whereas the total mass of the exposures did not correlate with increases in genotoxicity. The fact that the Primary and Fresh exposures had almost 4-fold difference in total mass (higher in the Primary test point) and the Fresh exposure still resulted in considerably higher genotoxicity, support the conclusion that the genotoxicity was not significantly dependent on the total mass.

In addition to the organic coating, SA is an important factor when considering toxicity (Schmid and Stoeger, 2016; Oberdörster et al., 2005), as the organic compounds on the particle SA are in direct contact with the exposed cells, thus, affecting what kind of compounds can distress the cells,

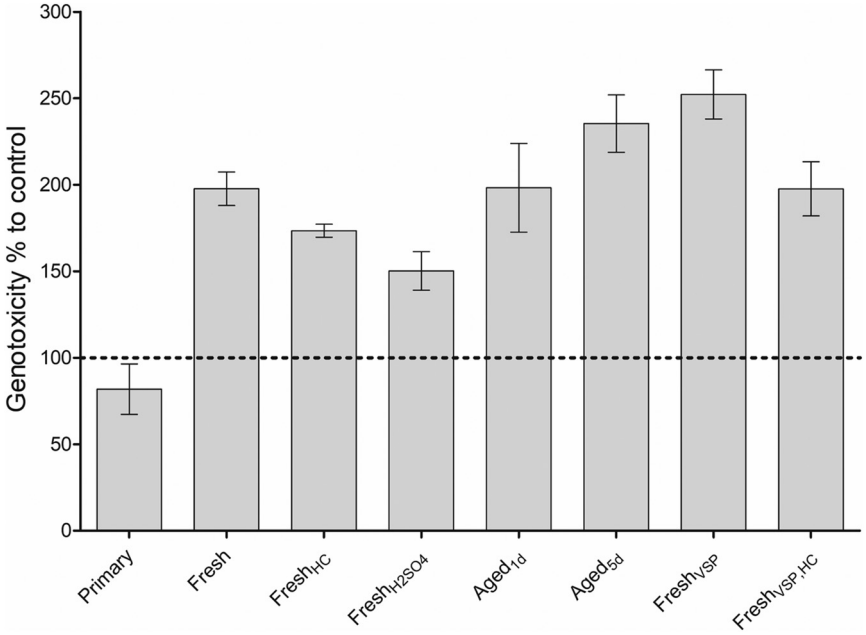

Fig. 3. Percent of genotoxicity compared to the clean air control, measured with Comet assay from differently treated BC exposures. Dashed line indicates the clean air control. Results are shown as geometric means ($n = 3$) with SEM.

and how the different effects can happen between the cells and toxic components. The SA is also one reason why the toxicity studies using CB do not represent the combustion originated BC, as the SA features between CB and BC differ; BC particles have more defects and therefore more surface functionalisation (Long et al., 2013). Moreover, the SA controls how much coating material can bind to the particles. Even though, phagocytic behaviour of A549 cells is negligible, it has been shown that particles containing surface absorbed organics, such as PAHs, can work outside of the cells as uptake reservoirs for these compounds, thus exerting toxicity to the cells even if the particle location is not intracellular (Liu et al., 2021).

With the two Aged exposures, the concentration of ozone was relatively high, especially in the Aged$_{5d}$. Ozone is known to induce oxidative stress and has been linked to genotoxicity with even lower concentrations than those observed in the present study (Poma et al., 2017). The role of the organics as the genotoxicity culprit is not undermined, however, as there were negligible levels of ozone in the three different Fresh exposures, still resulting in genotoxicity. Subsequently, ozone might have only increased the genotoxicity of both Aged exposures. Similarly to ozone, the both Aged samples also had CO, whereas, the rest of the samples did not. However, CO has not been associated with genotoxicity (Zhang et al., 2019). Both gases are a result of the aerosol aging setup, where ozone is added to simulate atmospheric conditions and CO is used as a tracer gas to calculate the age of the aerosol.

The VSP-G1 originated samples resulted in overall higher genotoxicity compared to the GB produced aerosol exposures, which is somewhat contrary

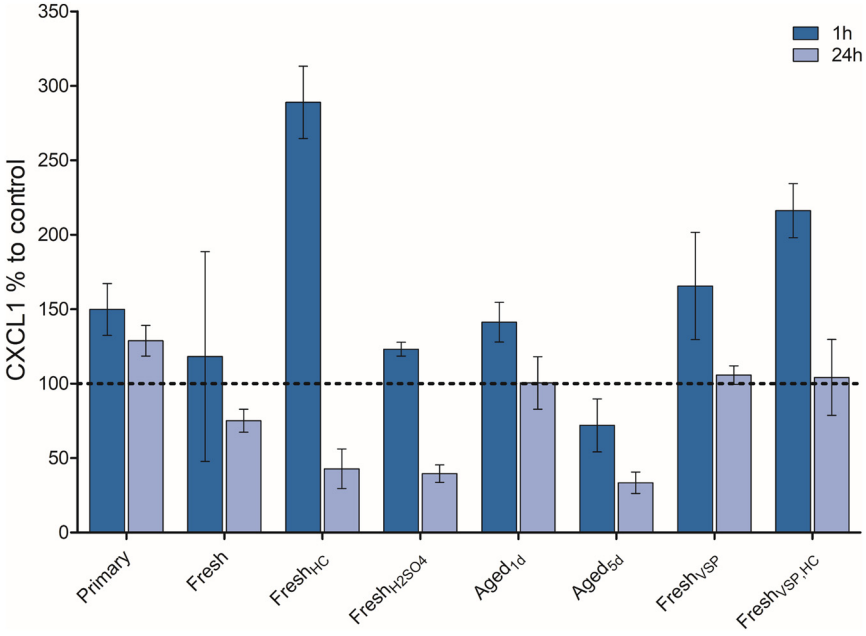

Fig. 4. Percent of CXCL-1 levels compared to the clean air control, measured with ELISA assay from differently treated BC exposures 1 h and 24 h after the exposures. Dashed line indicates the clean air control. Results are shown as geometric means ($n = 3$) with SEM.

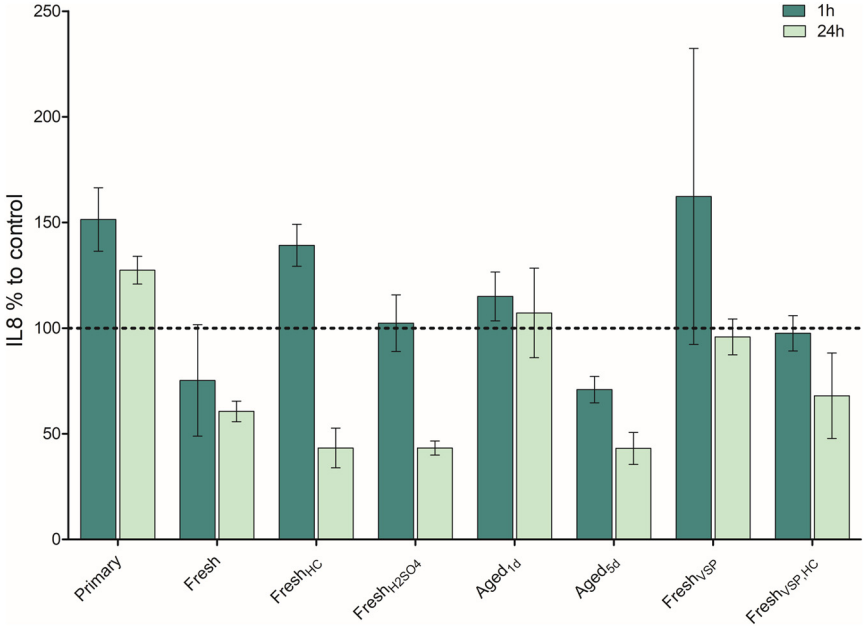

Fig. 5. Percent of IL-8 levels compared to the clean air control, measured with ELISA assay from differently treated BC exposures 1 h and 24 h after the exposures. Dashed line indicates the clean air control. Results are shown as geometric means (n = 3) with SEM.

to the organic coating hypothesis, as VSP-G1 originated samples had very little organic mass. Moreover, the total mass concentrations with VSP-G1 samples were also considerably lower compared to the GB samples. The underlying reason for increase in genotoxicity, however, might be the PM size as the VSP-G1 originated particles were especially small. Similarly, the study of Diabaté et al., 2021 observed genotoxicity and inflammatory responses in similar co-culture due exposure of low dose of nanoparticles in ALI. The particle mass concentration may also be somewhat underestimated, as the SP-AMS transmission efficiency is low for particles below 40 nm. Smaller particle size correlated with increased genotoxicity in both GB and VSP-G1 MMM models (not statistically in VSP-G1) and the effect of size on genotoxicity is plausible, as smaller particles can carry more surface compounds per a unit of mass, and penetrate deeper to the cells (Besis et al., 2017). One possible explanation for the high genotoxicity of VSP-G1 exposures compared to corresponding GB exposures might be the particle localization inside of the cell nucleus. It has been shown that SiO_2 nanoparticles with size fraction of 40 nm to 70 nm can be localized inside the nucleus of A549 cells (Chen and von Mikecz, 2005). Furthermore, a study by Perde-Schrepler et al. (2019) showed that Ag nanoparticles can be transported inside of the cell nucleus, which was associated with increase in genotoxicity. Even though both of these studies used different particles than our study, both SiO_2 and Ag nanoparticles are insoluble and have a low organic fraction as do the VSP-G1 particles. The small particle size as culprit of genotoxicity have been speculated in the previous studies using the thermophoresis-based ALI system (Ihantola et al., 2020; Ihantola et al., 2022). The particle size might also explain the difference in genotoxicity between the two VSP-G1 generated exposures, as the addition of HC increased particle size and lowered genotoxicity. Moreover, the genotoxicity seen from the GB samples might be higher than observed with the Comet assay, as the possible PAH DNA adducts may decrease the DNA tails due to the increased size of the DNA fragments (Kamal et al., 2015). Consequently, the organic coating might induce overall higher genotoxicity than the PM size.

Levels of CXCL1 and IL8 after 24 h from several GB samples decreased compared to the clean air control. This indicates immunosuppression

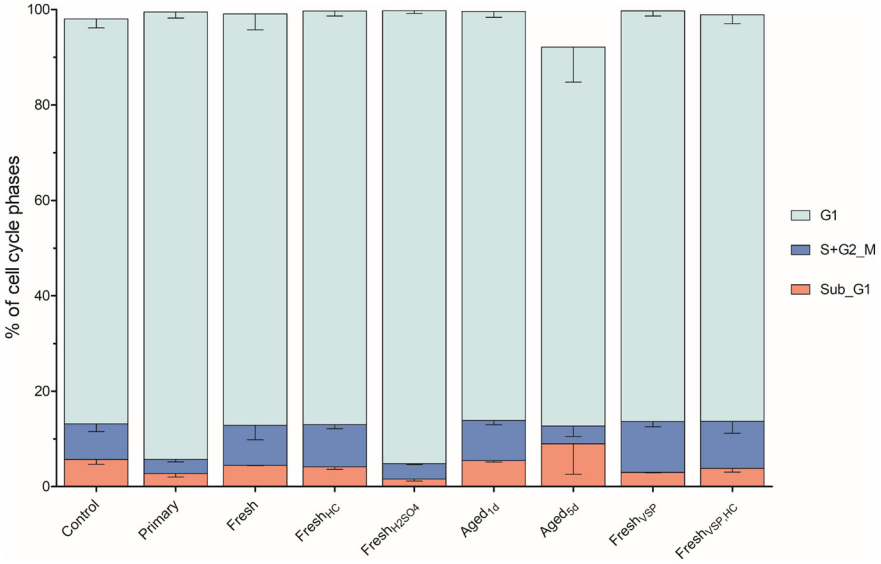

Fig. 6. Percent of different cell cycle phase populations from each exposure and clean air control. Results are shown as geometric means (n = 3) with SEM.

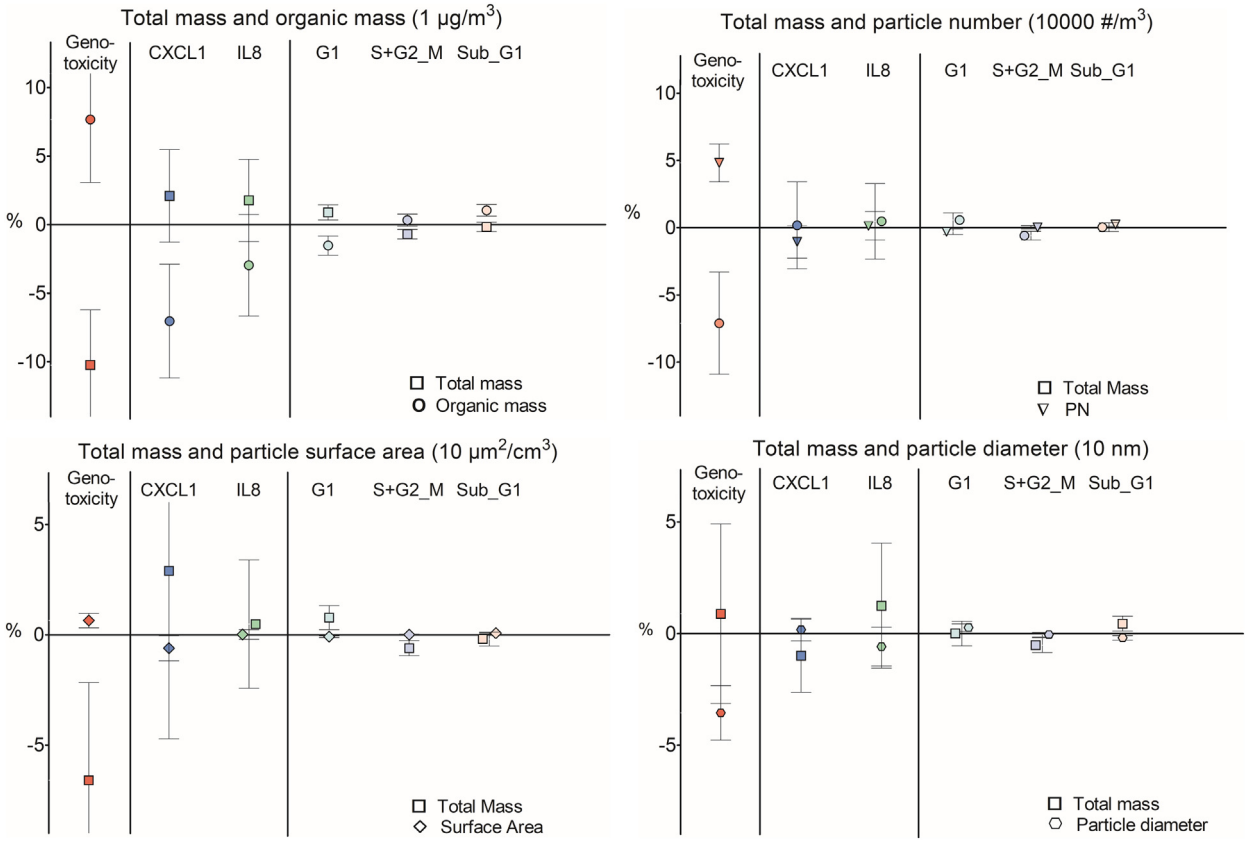

Fig. 7. Results of MMM analysis for GB originating samples. Different colours indicate distinct toxicological analysis and shapes aerosol components. Estimates indicates how much change of certain unit of aerosol component affects the toxicological responses. Units for total mass and organic mass, PN, SA and particle diameter are 1 μg/m^3, 10,000#/cm^3, 10 μm/cm^3, and 10 nm, respectively. $N = 3$ and 95 % CI.

due to aerosol exposure, as has been previously seen in multiple different cells and *in vivo* studies using urban and biomass combustion aerosol exposures (Martikainen et al., 2018; Jalava et al., 2009; Happo et al., 2013). Immunosuppression may indicate that the cellular process has been damaged in a way that the cells are incapable of producing defensive mechanisms anymore. Compared to the genotoxicity results, there were considerably less statistically significant results in the MMM analysis for CXCL1 and IL8. However, in both 24 h samples, decreasing particle size and increasing BC mass raised inflammatory mediator levels. Moreover, with CXCL1, an increase of organic mass was found to decrease the chemokine levels, supporting the hypothesis of high levels of organic compounds being a likely cause for immunosuppression. Previous studies have also linked PAHs to immunosuppression (Li et al., 2010; Ihantola et al., 2020; Ihantola et al., 2022), and PAHs exert their toxicity mainly through genotoxic pathways, such as bulky adducts and DNA strand breaks, which lead to cell cycle arrest and apoptosis (Gao et al., 2008). Thus, in our study the immunosuppression is a consequence of the genotoxicity, of what are presumed PAH compounds on the BC particle surfaces. This further emphasizes the toxicity of organics in the case of the GB exposures.

The higher CXCL1 and IL8 levels with 1 h samples compared to the 24 h samples are logical, as cells start to produce inflammatory mediators immediately at the exposure, but the possible PAH DNA adduct formation which leads to immunosuppression occurs after some time (Genies et al., 2013). An exception is the Aged$_{5d}$ exposure, however, as the chemokine production was suppressed in both CXCL1 and IL8 1 h samples, indicating high immunotoxicity already during the exposure. Moreover, the 1 h result show that Fresh$_{HC}$ increases CXCL1 production up to 3-fold compared to clean air control; the octacosane coating possibly having an important part in this. However, this will stay only as speculation due to the lack of studies concerning immunotoxicity of saturated hydrocarbons.

Concerning the VSP-G1 originated samples, the 24 h CXCL1 and IL8 results were comparable to the control. However, from the 1 h samples, an increase in both CXCL1 and IL8 levels compared to control indicate that exposures raised inflammation in cells immediately after the exposure, but that the inflammation levels were decreased back to control levels after 24 h. An interesting aspect is the possible effect of particle size, which increased genotoxicity in VSP-G1 exposures, apparently did not initiate immunosuppression. It might be that the observed genotoxicity in VSP-G1 aerosol exposed cells did not yet compromise the cellular processes. This is in line with the speculation that the genotoxicity seen in VSP-G1 samples is primary genotoxicity, in which the inflammation is negligible (Schins and Knaapen, 2007).

Within the cell cycle analysis, the G1 indicate cell growth, the S + G2_M indicate the state of cell mitosis, and the Sub_G1 phase indicates the state of apoptosis. Thus, the cell phase differences between the clean air control and exposures are a sign of damage to the cell cycle from the aerosol exposures. PM exposure has been previously linked to the disturbance of the cell cycle as well (Xiao et al., 2019), and to the organic fraction of PM and its genotoxicity (Longhin et al., 2013). Our results show differences in cell phases compared to the clean air control in all except the GB Fresh and Fresh$_{HC}$ exposures. The highest Sub_G1 levels were detected in the Aged$_{5d}$ exposure, which is in line with the other toxicological responses to this exposure, as increases in Sub G1 phase indicate extensive DNA degradation connected to apoptosis (Bai et al., 2017). This result also points to the genotoxicity of the organic fraction within the exposures, similarly as seen in the study by Longhin et al. (2013). The MMM analysis supports this with a statistically significant decrease of G1 phase and increase of Sub_G1 phase associated with organic mass. The high G1 levels indicate that the cell proliferation has stopped, which was seen in the samples of Primary and Fresh$_{H2SO4}$, indicating that cells may be switching focus from division to, for example, defensive processes. This is line with the high inflammation and low genotoxicity seen in

the Primary samples. For the $Fresh_{H2SO4}$, the genotoxicity results were the second lowest, thus also being somewhat in line with the high levels of cells in G1 phase. Furthermore, with the VSP-G1 samples, there was a low amount of cells in Sub_G1 phase, but quite a high amount of cells in S + G2_M cell cycle phase, suggesting cell cycle arrest at G2/M phase, which could lead to prolonged cell damage and halting of cell growth (Yang et al., 2018).

Limitations of this study were the use of relatively few toxicological analyses, due to conducting the exposures in a combustion aerosol lab rather than a toxicological laboratory space. Thus, the assays were restricted mainly to those in which cells could be collected and stored for later analyses. The future studies using more toxicological analyses and variation of different cell lines, with addition of even primary cells, should be considered. Furthermore, PAH measurements would have been a great addition for deeper discussion of the possible toxicity of organic coatings. Additionally, the *in vitro* system is (as always) only a rough estimation of a whole human, thus, results cannot be perfectly linked to health effects in humans and to wider public health. Especially the lung deposition differs from the deposition within our ALI system. With some uncertainties, the particle size range of few hundred to several hundred nm is less likely to deposit to the lung alveolar region, compared to the particles with size range of tens of nm (Löndahl et al., 2014). Whereas, in the thermophoresis-based ALI system, the deposition stays quite constant from UFP size range up to particles with 1 μm diameter, therefore reducing the representativeness of the reported outcome for human risk evaluation. The methodology of the test aerosol production in this study could have been improved. As discussed in the results section, we had some difficulties with the soot production. In future studies, more effort should go towards controlling the primary soot size and concentration. Additionally, it would be beneficial from a statistics perspective to include more size variation within each sample treatment group in order to distinguish between effects due to particle size and sample treatment. Future studies should also look at particle morphology, as it is known that BC can be emitted in a highly fractal structure, which influences the uptake of semivolatile vapours. Finally, a simple control for effects due to gases (instead of particles) should be included in future studies, by removing particles using a high-efficiency particulate filter (HEPA filter).

The domestic energy generation and biomass burning were found as the most important sources connected to health effects of BC in the recent study of Chowdhury et al. (2022). Furthermore, the sources of BC can also affect the coating of the BC particles, with solid fuel combustion resulting to particles with higher coating compared to the traffic emissions (Liu et al., 2017). Additionally, the environmental aspects, such as season can also affect the coating of the BC particles, with for example photo-oxidation enchanting the secondary aerosols (Liu et al., 2019a, 2019b). Consequently, these studies are pinpointing the importance of reducing the impacts of biomass combustion.

Our study, as far as we are aware, is one of the very first toxicological studies using real combustion originated BC aerosols. BC as a PM component is an interesting focus of the toxicological studies, as it has been argued that BC is a relatively more hazardous component of the whole PM aerosol (Janssen et al., 2011; Yang et al., 2021). The hypothesis for higher toxicity has been suggested to be caused by the high carbon content of BC, the small particle size, and the large surface area which acts as a condensation sink for organic vapours (Grahame et al., 2014). Our results agree with two of the suggested properties: particle size and organic fraction. The results indicate that organic coating and atmospheric aging of the BC particles increases their toxicity, as seen in multiple different exposures within our study and accentuated by the results of the statistical analyses. Moreover, the recent study of Offer et al., 2022 using ALI exposure system with co-culture, showed that the aged soot particles induced higher genotoxicity and inflammatory effects, compared to the primary particles, thus, showing very similar results as the present study. Moreover, the smaller particle size correlated with increased toxicity, seen especially with VSP-G1 originated aerosol exposures. Therefore, in addition to BC, the results of our study emphasize the role of UFP emissions and their possible effect on public health. Levels of UFP in the environment have not been significantly decreasing in recent years (Presto et al., 2021), thus, supporting the recent statement by the WHO (WHO, 2021) that UFP levels should be added to monitoring measurements. Overall mitigation of air pollution with aims of both global climate change and air quality improvements are important, and BC as mitigation focus affects both (Harmsen et al., 2020).

5. Conclusions

In the present study, we conducted *in vitro* exposures of combustion originated BC with novel thermophoresis-based ALI system. The different aerosol treatments induced various physical and chemical aerosol characteristics which affected the toxicity of the primary, fresh and aged aerosol particles. Aged aerosols typically consist of particles with a higher concentration of organics, compared to primary or freshly emitted aerosols. The VSP-G1 spark generator was included in the study as a different source of aerosols. Results from the GB exposures emphasized the importance of the organic coating to genotoxicity and immunosuppression, and the VSP-G1 exposures emphasized the genotoxicity of the ultra-fine particulates. Therefore, the overall drivers of the toxicity seemed to be the organic fraction and the particle size of the aerosols. Both were further emphasized by the statistical analyses. Despite the imperfect representativeness of the *in vitro* system compared to whole human exposure, the results of the present study suggest that the BC emission reduction should focus on combustion emissions with small particle sizes or simultaneous organic emissions for the largest benefits to air quality.

CRediT authorship contribution statement

All authors contributed to writing the manuscript and approved the present version.

Performed experimental work: Henri Hakkarainen, Laura Salo, Sanna Saarikoski, Minna Aurela, Kimmo Teinilä, Sampsa Martikainen, Petteri Marjanen, Teemu Lepistö, Niina Kuittinen, Pasi I Jalava.

Evaluated data: Henri Hakkarainen, Laura Salo, Santtu Mikkonen, Sanna Saarikoski, Minna Aurela, Kimmo Teinilä, Mika Ihalainen, Sampsa Martikainen, Petteri Marjanen, Teemu Lepistö, Karri Saarnio, Hilkka Timonen, Niina Kuittinen, Topi Rönkkö, Pasi I Jalava.

Provided experimental and instrumental infrastructure: Karri Saarnio, Tobias V. Pfeiffer, Hilkka Timonen, Topi Rönkkö, Pasi I Jalava.

Wrote and edited the manuscript: Henri Hakkarainen, Laura Salo, Santtu Mikkonen, Sanna Saarikoski, Minna Aurela, Kimmo Teinilä, Mika Ihalainen, Sampsa Martikainen, Petteri Marjanen, Teemu Lepistö, Karri Saarnio, Hilkka Timonen, Tobias V. Pfeiffer, Niina Kuittinen, Topi Rönkkö, Pasi I Jalava.

Declaration of competing interest

The authors declare that they have no known competing financial interests or personal relationships that could have appeared to influence the work reported in this paper. Tobias V Pfeiffer has employment at VSParticle, who provided instrument, but however did not participate to the measurements or the data analysis.

Acknowledgements

Vaisala provided electrochemical gas sensors for this study and conducted initial analysis of the gas data and Dekati provided one ELPI+ to be used in the measurements. VSParticle provided the spark generator used in two of the test points.

Funding

Financial support from Black Carbon Footprint project funded by Business Finland (grant nr: 528/31/2019, 530/31/2019), participating companies and municipal actors. Academy of Finland Flagship Programme “ACCC” (Grant numbers 337550, 337551, 337552) and the Academy of Finland competitive funding to strengthen university research profiles (PROFI) for the University of Eastern Finland (grant No. 325022), with addition of University of Eastern Finland doctoral school EPHB funding, are gratefully acknowledged.

This project has received funding from the European Union's Horizon 2020 research and innovation programme under grant agreement No 814978 (TUBE).

Appendix A. Supplementary data

Supplementary data to this article can be found online at https://doi.org/10.1016/j.scitotenv.2022.156543.

References

Adams, K., Greenbaum, D.S., Shaikh, R., van Erp, A.M., Russell, A.G., 2015. Particulate matter components, sources, and health: systematic approaches to testing effects. J. Air Waste Manage. Assoc. 65 (5), 544–558. https://doi.org/10.1080/10962247.2014.1001884.

Anon, 2021. WHO global air quality guidelines. Particulate Matter (PM2.5 and PM10), Ozone, Nitrogen Dioxide, Sulfur Dioxide and Carbon Monoxide. World Health Organization, Geneva Licence: CC BY-NC-SA 3.0 IGO.

Bai, H., Wu, M., Zhang, H., Tang, G., 2017. Chronic polycyclic aromatic hydrocarbon exposure causes DNA damage and genomic instability in lung epithelial cells. Oncotarget 8 (45), 79034–79045. https://doi.org/10.18632/oncotarget.20891 Published 2017 Sep 15.

Bates, D., Maechler, M., Bolker, B., Walker, S., 2015. Fitting linear mixed-effects models using lme4. J. Stat. Softw. 67 (1), 1–48. https://doi.org/10.18637/jss.v067.i01.

Besis, A., Tsolakidou, A., Balla, D., Samara, C., Voutsa, D., Pantazaki, A., Choli-Papadopoulou, T., Lialiaris, T.S., 2017. Toxic organic substances and marker compounds in size-segregated urban particulate matter - implications for involvement in the in vitro bioactivity of the extractable organic matter. Environ. Pollut. 230, 758–774. https://doi.org/10.1016/j.envpol.2017.06.096.

Billet, S., Landkocz, Y., Martin, P.J., Verdin, A., Ledoux, F., Lepers, C., André, V., Cazier, F., Sichel, F., Shirali, P., Gosset, P., Courcot, D., 2018. Chemical characterization of fine and ultrafine PM, direct and indirect genotoxicity of PM and their organic extracts on pulmonary cells. Journal of Environmental Sciences (ISSN: 1001-0742) 71, 168–178. https://doi.org/10.1016/j.jes.2018.04.022.

Boeije, Maurits F.J., Biskos, George, van der Maesen, Bibianne E., Pfeiffer, Tobias V., van Vugt, Aaike W., Zijlstra, Bernardus, Schmidt-Ott, A., 2020. Nanoparticle production by spark ablation: principle, configurations, and basic steps toward application. Spark Ablation. Jenny Stanford Publishing.

Bond, T.C., Doherty, S.J., Fahey, D.W., Forster, P.M., Berntsen, T., DeAngelo, B.J., Flanner, M.G., Ghan, S., Kärcher, B., Koch, D., Kinne, S., Kondo, Y., Quinn, P.K., Sarofim, M.C., Schultz, M.G., Schulz, M., Venkataraman, C., Zhang, H., Zhang, S., Bellouin, N., Guttikunda, S.K., Hopke, P.K., Jacobson, M.Z., Kaiser, J.W., Klimont, Z., Lohmann, U., Schwarz, J.P., Shindell, D., Storelvmo, T., Warren, S.G., Zender, C.S., 2013. Bounding the role of black carbon in the climate system: a scientific assessment. J. Geophys. Res. Atmos. 118, 5380–5552. https://doi.org/10.1002/jgrd.50171.

Borrás, E., Luis Tortajada-Genaro, L., 2012. Secondary organic aerosol formation from the photo-oxidation of benzene. Atmospheric Environment 47, 154–163. https://doi.org/10.1016/j.atmosenv.2011.11.020.

Cai, J., Chu, B., Yao, L., Yan, C., Heikkinen, L.M., Zheng, F., Li, C., Fan, X., Zhang, S., Yang, D., Wang, Y., Kokkonen, T.V., Chan, T., Zhou, Y., Dada, L., Liu, Y., He, H., Paasonen, P., Kujansuu, J.T., Petäjä, T., Mohr, C., Kangasluoma, J., Bianchi, F., Sun, Y., Croteau, P.L., Worsnop, D.R., Kerminen, V.-M., Du, W., Kulmala, M., Daellenbach, K.R., 2020. Size-segregated particle number and mass concentrations from different emission sources in urban Beijing. Atmos. Chem. Phys. 20, 12721–12740. https://doi.org/10.5194/acp-20-12721-2020.

Cassee, F.R., Héroux, M.E., Gerlofs-Nijland, M.E., Kelly, F.J., 2013. Particulate matter beyond mass: recent health evidence on the role of fractions, chemical constituents and sources of emission. Inhal. Toxicol. 25, 802–812. https://doi.org/10.3109/08958378.2013.850127.

Chen, M., von Mikecz, A., 2005. Formation of nucleoplasmic protein aggregates impairs nuclear function in response to SiO2 nanoparticles. Exp.Cell Res. 305, 51–62.

Chowdhury, S., Pozzer, A., Haines, A., Klingmüller, K., Münzel, T., Paasonen, P., Sharma, A., Venkataraman, C., Lelieveld, J., 2022. Global health burden of ambient PM2.5 and the contribution of anthropogenic black carbon and organic aerosols. Environment International (ISSN: 0160-4120) 159, 107020. https://doi.org/10.1016/j.envint.2021.107020.

Diabaté, S., Armand, L., Murugadoss, S., Dilger, M., Fritsch-Decker, S., Arnal, M.-E., Biola-Clier, M., Ambrose, S., et al., Schlager, C., Béal, D., 2021. Air–liquid interface exposure of lung epithelial cells to low doses of nanoparticles to assess pulmonary adverse effects. Nanomaterials 11, 65. https://doi.org/10.3390/nano11010065.

Drinovec, L., Močnik, G., Zotter, P., Prévôt, A.S.H., Ruckstuhl, C., Coz, E., Rupakheti, M., Sciare, J., Müller, T., Wiedensohler, A., Hansen, A.D.A., 2015. The "dual-spot" aethalometer: an improved measurement of aerosol black carbon with real-time loading compensation. Atmos. Meas. Tech. 8, 1965–1979. https://doi.org/10.5194/amt-8-1965-2015.

Enroth, J., Saarikoski, S., Niemi, J., Kousa, A., Ježek, I., Močnik, G., Carbone, S., Kuuluvainen, H., Rönkkö, T., Hillamo, R., Pirjola, L., 2016. Chemical and physical characterization of traffic particles in four different highway environments in the Helsinki metropolitan area. Atmos. Chem. Phys. 16 (9), 5497–5512. https://doi.org/10.5194/acp-16-5497-2016.

EPA, U.S., 2012. Report to Congress on Black Carbon. US Environmental Protection Agency, Washington, DC EPA-450/R-12-001.

Gao, J., Mitchell, L.A., Lauer, F.T., Burchiel, S.W., 2008. p53 and ATM/ATR regulate 7,12-dimethylbenz[a]anthracene-induced immunosuppression. Molecular Pharmacology 73 (1), 137–146. https://doi.org/10.1124/mol.107.039230 January 1.

Genies, C., Maître, A., Lefèbvre, E., Jullien, A., Chopard-Lallier, M., et al., 2013. The extreme variety of genotoxic response to Benzo[a]pyrene in three different human cell lines from three different organs. PLOS ONE 8 (11), e78356. https://doi.org/10.1371/journal.pone.0078356.

Genies, C., Jullien, A., Lefebvre, E., Revol, M., Maitre, A., Douki, T., 2016. Inhibition of the formation of benzo[a]pyrene adducts to DNA in A549 lung cells exposed to mixtures of polycyclic aromatic hydrocarbons. Toxicol. Vitro 35, 1–10. https://doi.org/10.1016/j.tiv.2016.05.006.

Grahame, T.J., Klemm, R., Schlesinger, R.B., 2014. Public health and components of particulate matter: the changing assessment of black carbon. J. Air Waste Manage. Assoc. 64 (6), 620–660. https://doi.org/10.1080/10962247.2014.912692.

Gramsch, E., Muñoz, A., Langner, J., Morales, L., Soto, C., Pérez, P., Rubio, M.A., 2020. Black carbon transport between Santiago de Chile and glaciers in the Andes Mountains. Atmospheric Environment (ISSN: 1352-2310) 232, 117546. https://doi.org/10.1016/j.atmosenv.2020.117546.

Hansen, A.D.A., Rosen, H., Novakov, T., 1984. The aethalometer — an instrument for the real-time measurement of optical absorption by aerosol particles. Sci. Total Environ. 36, 191–196. https://doi.org/10.1016/0048-9697(84)90265-1.

Happo, M.S., Uski, O., Jalava, P.I., et al., 2013. Pulmonary inflammation and tissue damage in the mouse lung after exposure to PM samples from biomass heating appliances of old and modern technologies. Sci. Total Environ. 443, 256–266.

Hara, K., Sudo, K., Ohnishi, T., Osada, K., Yabuki, M., Shiobara, M., Yamanouchi, T., 2019. Seasonal features and origins of carbonaceous aerosols at Syowa Station, coastal Antarctica. Atmos. Chem. Phys. 19, 7817–7837. https://doi.org/10.5194/acp-19-7817-2019V.I.

Harmsen, M., et al., 2020. Co-benefits of black carbon mitigation for climate and air quality. Clim. Chang. https://doi.org/10.1007/s10584-020-02800-8.

Heikkilä, J., Virtanen, A., Rönkkö, T., Keskinen, J., Aakko-Saksa, P., Murtonen, T., 2009. Nanoparticle emissions from a heavy-duty engine running on alternative diesel fuels. Environ. Sci. Technol. 43 (24), 9501–9506. https://doi.org/10.1021/es9013807.

Ihalainen, M., Jalava, P., Ihantola, T., Kasurinen, S., Uski, O., Sippula, O., Hartikainen, A., Tissari, J., Kuuspalo, K., Lähde, A., Hirvonen, M.-R., Jokiniemi, J., 2019. Design and validation of an air-liquid interface (ALI) exposure device based on thermophoresis. Aerosol Sci. Technol. 53 (2), 133–145. https://doi.org/10.1080/02786826.2018.1556775.

Ihantola, T., Di Bucchianico, S., Happo, M., et al., 2020. Influence of wood species on toxicity of log-wood stove combustion aerosols: a parallel animal and air-liquid interface cell exposure study on spruce and pine smoke. Part Fibre Toxicol. 17, 27. https://doi.org/10.1186/s12989-020-00355-1.

Ihantola, T., Hirvonen, M.R., Mika Ihalainen, M., et al., 2022. Genotoxic and inflammatory effects of spruce and brown coal briquettes combustion aerosols on lung cells at the air-liquid interface. Science of The Total Environment (ISSN: 0048-9697) 806 (1), 150489. https://doi.org/10.1016/j.scitotenv.2021.150489.

Jalava, P.I., Hirvonen, M.R., Sillanpää, M., et al., 2009. Associations of urban air particulate composition with inflammatory and cytotoxic responses in RAW 246.7 cell line. Inhal. Toxicol. 21 (12), 994–1006.

Janssen, N.A., Hoek, G., Simic-Lawson, M., Fischer, P., van Bree, L., ten Brink, H., Keuken, M., Atkinson, R.W., Anderson, H.R., Brunekreef, B., Cassee, F.R., 2011 Decc. Black carbon as an additional indicator of the adverse health effects of airborne particles compared with PM10 and PM2.5. Environ. Health Perspect. 119 (12), 1691–1699. https://doi.org/10.1289/ehp.1003369.

Janssen, N.A., Gerlofs-Nijland, M.E., Lanki, T., Salonen, R.O., Cassee, F., Hoek, G., et al., 2012. Health Effects of Black Carbon. World Health Organization, Copenhagen.

Järvinen, A., Aitomaa, M., Rostedt, A., Keskinen, J., Yli-Ojanperä, J., 2014. Calibration of the new electrical low pressure impactor (ELPI+). J. Aerosol Sci. 69, 150–159. https://doi.org/10.1016/j.jaerosci.2013.12.006.

Kahnert, M., 2017. Optical properties of black carbon aerosols encapsulated in a shell of sulfate: comparison of the closed cell model with a coated aggregate model. Opt. Express 25, 24579–24593. https://doi.org/10.1364/OE.25.024579.

Kamal, A., Cincinelli, A., Martellini, T., Malik, R.N., 2015. A review of PAH exposure from the combustion of biomass fuel and their less surveyed effect on the blood parameters. Environ. Sci. Pollut. Res. 22, 4076–4098. https://doi.org/10.1007/s11356-014-3748-0.

Kanashova, Tamara, et al., 2018. Emissions from a modern log wood masonry heater and wood pellet boiler: composition and biological impact on air-liquid interface exposed human lung cancer cells. J. Mol. Clin. Med. 1 (1), 23.

Kang, E., Root, M.J., Toohey, D.W., Brune, W.H., 2007. Introducing the concept of potential aerosol mass (PAM). Atmos. Chem. Phys. 7, 5727–5744. https://doi.org/10.5194/acp-7-5727-2007.

Karjalainen, P., Pirjola, L., Heikkilä, J., Lähde, T., Tzamkiozis, T., Ntziachristos, L., Keskinen, J., Rönkkö, T., 2014. Exhaust particles of modern gasoline vehicles: A laboratory and an on-road study. Atmospheric Environment (ISSN: 1352-2310) 97, 262–270. https://doi.org/10.1016/j.atmosenv.2014.08.025.

Karjalainen, P., Saari, S., Kuuluvainen, H., Kalliohaka, T., Taipale, A., Rönkkö, T., 2017. Performance of ventilation filtration technologies on characteristic traffic related aerosol down to nanocluster size. Aerosol Sci. Technol. 51 (12), 1398–1408. https://doi.org/10.1080/02786826.2017.1356904.

Keskinen, J., Rönkkö, T., 2010. Can real-world diesel exhaust particle size distribution be reproduced in the Laboratory? A Critical Review Jorma Keskinen. Journal of the Air & Waste Management Association 60 (10), 1245–1255. https://doi.org/10.3155/1047-3289.60.10.1245.

Keskinen, J., Pietarinen, K., Lehtimäki, M., 1992. Electrical low pressure impactor. J. Aerosol Sci. 23 (4), 353–360.

Kirrane, E.F., Luben, T.J., Benson, A., Owens, E.O., Sacks, J.D., Dutton, S.J., Madden, M., Nichols, J.L., 2019 Junn. A systematic review of cardiovascular responses associated with ambient black carbon and fine particulate matter. Environ. Int. 127, 305–316. https://doi.org/10.1016/j.envint.2019.02.027.

Kostenidou, E., Martinez-Valiente, A., R'Mili, B., Marques, B., Temime-Roussel, B., Durand, A., André, M., Liu, Y., Louis, C., Vansevenant, B., Ferry, D., Laffon, C., Parent, P., D'Anna, B., 2021. Technical note: emission factors, chemical composition, and morphology of particles emitted from euro 5 diesel and gasoline light-duty vehicles during transient cycles. Atmos. Chem. Phys. 21 (6), 4779–4796. https://doi.org/10.5194/acp-21-4779-2021.

Lambe, A.T., Ahern, A.T., Williams, L.R., Slowik, J.G., Wong, J.P.S., Abbatt, J.P.D., Brune, W.H., Ng, N.L., Wright, J.P., Croasdale, D.R., Worsnop, D.R., Davidovits, P., Onasch,

T.B., 2011. Characterization of aerosol photooxidation flow reactors: heterogeneous oxidation, secondary organic aerosol formation and cloud condensation nuclei activity measurements. Atmos. Meas. Tech. 4, 445–461. https://doi.org/10.5194/amt-4-445-2011.

Li, Q., Lauer, F.T., Liu, K.J., Hudson, L.G., Burchiel, S.W., 2010. Low-dose synergistic immunosuppression of T-dependent antibody responses by polycyclic aromatic hydrocarbons and arsenic in C57BL/6J murine spleen cells. Toxicol. Appl. Pharmacol. 245, 344–351. https://doi.org/10.1016/j.taap.2010.03.020.

Liu, D., Whitehead, J., Alfarra, M., et al., 2017. Black-carbon absorption enhancement in the atmosphere determined by particle mixing state. Nat. Geosci. 10, 184–188. https://doi.org/10.1038/ngeo2901.

Liu, D., Joshi, R., Wang, J., Yu, C., Allan, J.D., Coe, H., Flynn, M.J., Xie, C., Lee, J., Squires, F., Kotthaus, S., Grimmond, S., Ge, X., Sun, Y., Fu, P., 2019. Contrasting physical properties of black carbon in urban Beijing between winter and summer. Atmos. Chem. Phys. 19, 6749–6769. https://doi.org/10.5194/acp-19-6749-2019.

Liu, D., Zhao, D., Xie, Z., Yu, C., Chen, Y., Tian, P., Ding, S., Hu, K., Lowe, D., Liu, Q., Zhou, W., Wang, F., Sheng, J., Kong, S., Hu, D., Wang, Z., Huang, M., Ding, D., 2019. Enhanced heating rate of black carbon above the planetary boundary layer over megacities in summertime. environ, resLett. 14, 124003. https://doi.org/10.1088/1748-9326/ab4872.

Liu, X., Ma, J., Ji, R., Wang, S., Zhang, Q., Zhang, C., Liu, S., Chen, W., 2021. Biochar fine particles enhance uptake of Benzo(a)pyrene to macrophages and epithelial cells via different mechanisms. Environ. Sci. Technol. Lett. 8 (3), 218–223. https://doi.org/10.1021/acs.estlett.0c00900.

Löndahl, J., Möller, W., Pagels, J.H., Kreyling, W.G., Swietlicki, E., Schmid, O., Aug 2014. Journal of Aerosol Medicine and Pulmonary Drug Delivery, 229–254 https://doi.org/10.1089/jamp.2013.1044.

Long, C.M., Nascarella, M.A., Valberg, P.A., 2013. Carbon black vs. black carbon and other airborne materials containing elemental carbon: physicaland chemical distinctions. Environmental Pollution (ISSN: 0269-7491) 181, 271–286. https://doi.org/10.1016/j.envpol.2013.06.009.

Longhin, E., Holme, J.A., Gutzkow, K.B., et al., 2013. Cell cycle alterations induced by urban PM2.5 in bronchial epithelial cells: characterization of the process and possible mechanisms involved. Part Fibre Toxicol. 10, 63. https://doi.org/10.1186/1743-8977-10-63.

Luoma, K., Niemi, J.V., Aurela, M., Fung, P.L., Helin, A., Hussein, T., Kangas, L., Kousa, A., Rönkkö, T., Timonen, H., Virkkula, A., Petäjä, T., 2021. Spatiotemporal variation and trends in equivalent black carbon in the Helsinki metropolitan area in Finland. Atmos. Chem. Phys. 21, 1173–1189. https://doi.org/10.5194/acp-21-1173-2021.

Martikainen, M.-V., Rönkkö, T.J., Schaub, B., et al., 2018. Integrating farm and air pollution studies in search for immunoregulatory mechanisms operating in protective and high-risk environments. Pediatr. Allergy Immunol. 29, 815–822. https://doi.org/10.1111/pai.12975.

Mathis, U., Ristimäki, J., Mohr, M., Keskinen, J., Ntziachristos, L., Samara, Z., Mikkanen, P., 2004. Sampling conditions for the measurement of nucleation mode particles in the exhaust of a diesel vehicle. Aerosol Sci. Technol. 38 (12), 1149–1160. https://doi.org/10.1080/027868290891497.

Mehtätalo, Lappi, 2020. Biometry for Forestry and Environmental Data: With Examples in R. CRC Press LLC, Boca Raton, FL.

Mikkonen, S., Korhonen, H., Romakkaniemi, S., Smith, J.N., Joutsensaari, J., Lehtinen, K.E.J., Hamed, A., Breider, T.J., Birmili, W., Spindler, G., Plass-Duelmer, C., Facchini, M.C., Laaksonen, A., 2011. Meteorological and trace gas factors affecting the number concentration of atmospheric aitken (Dp = 50 nm) particles in the continental boundary layer: parameterization using a multivariate mixed effects model. geosciModel Dev. 4, 1–13. https://doi.org/10.5194/gmd-4-1-2011.

Müller, J.O., Su, D.S., Wild, U., Schlögl, R., 2007 Aug 14. Bulk and surface structural investigations of diesel engine soot and carbon black. Phys. Chem. Chem. Phys. 9 (30), 4018–4025. https://doi.org/10.1039/b704850e.

Ntziachristos, L., Giechaskiel, B., Pistikopoulos, P., Samaras, Z., et al., 2004. Performance evaluation of a novel sampling and measurement system for exhaust particle characterization. SAE Technical Paper 2004-01-1439 https://doi.org/10.4271/2004-01-1439.

Oberdörster, G., Oberdörster, E., Oberdörster, J., 2005. Nanotoxicology: an emerging discipline evolving from studies of ultrafine particles. Environmental Health Perspectives (ISSN: 0091-6765) 113 (7), 823–839 July 2005.

Offer, S., Hartner, E., Bucchianico, S.D., Bisig, C., Bauer, S., Pantzke, J., Zimmermann, E.J., Cao, X., Binder, S., Kuhn, E., Huber, A., Jeong, S., Käfer, U., Martens, P., Mesceriakovas, A., Bendl, J., Brejcha, R., Buchholz, A., Gat, D., Hohaus, T., Rastak, N., Jakobi, G., Kalberer, M., Kanashova, T., Hu, Y., Ogris, C., Marsico, A., Theis, F., Pardo, M., Gröger, T., Oeder, S., Orasche, J., Paul, A., Ziehm, T., Zhang, Z., Adam, T., Sippula, O., Sklorz, M., Schnelle-Kreis, J., Czech, H., Kiendler-Scharr, A., Rudich, Y., Zimmermann, R., 2022. Effect of atmospheric aging on soot particle toxicity in lung cell models at the air–liquid interface: differential toxicological impacts of biogenic and anthropogenic secondary organic aerosols (SOAs). Environmental Health Perspectives 130 (2). https://doi.org/10.1289/EHP9413 CID: 027003.

Onasch, T.B., Trimborn, A., Fortner, E.C., Jayne, J.T., Kok, G.L., Williams, L.R., Davidovits, P., Worsnop, D.R., 2012. Soot particle aerosol mass spectrometer: development, validation, and initial application. Aerosol Sci. Technol. 46 (7), 804–817. https://doi.org/10.1080/02786826.2012.663948.

Perde-Schrepler, M., Florea, A., Brie, I., Virag, P., Fischer-Fodor, E., Vâlcan, A., Gurzău, E., Lisencu, C., Maniu, A.J., 2019. Size-dependent cytotoxicity and genotoxicity of silver nanoparticles in Cochlear cells in vitro. Nanomaterials 2019, 6090259. https://doi.org/10.1155/2019/6090259.

Poma, A., Colafarina, S., Aruffo, E., Zarivi, O., Bonfigli, A., Di Bucchianico, S., et al., 2017. Effects of ozone exposure on human epithelial adenocarcinoma and normal fibroblasts cells. PLoS ONE 12 (9), e0184519. https://doi.org/10.1371/journal.,pone.0184519.

Presto, A.A., Saha, P.K., Robinson, A.L., 2021. Past, present, and future of ultrafine particle exposures in North America. Atmospheric Environment: X (ISSN: 2590-1621) 10, 100109. https://doi.org/10.1016/j.aeaoa.2021.100109.

R Core Team, 2021. R: A Language and Environment for Statistical Computing. R Foundation for Statistical Computing, Vienna, Austria https://www.R-project.org/.

Ristimäki, J., et al., 2007. Hydrocarbon condensation in heavy-duty diesel exhaust. Environ. Sci. Technol. 41. https://doi.org/10.1021/es0624319.

Ritchie, H., Roser, M., 2017. Air Pollution. Retrieved fromOurWorldInData.org Online Resource https://ourworldindata.org/air-pollution.

Rönkkö, T., Virtanen, A., Kannosto, J., Keskinen, J., Lappi, M., Pirjola, L., 2007. Nucleation mode particles with a nonvolatile Core in the exhaust of a heavy duty diesel vehicle. Environ. Sci. Technol. 41 (18), 6384–6389. https://doi.org/10.1021/es0705339.

Rönkkö, T., et al., 2011. Diesel exhaust nanoparticle volatility studies by a new thermodenuder with low solid nanoparticle losses. 15th ETH Conf. on Combust. Gener. Nanoparticles.

Rönkkö, T.J., Hirvonen, M.V., Happo, M.S., Ihantola, T., Hakkarainen, H., Martikainen, M.-V., Gu, C., Wang, Q., Jokiniemi, J., Komppula, M., Jalava, P.I., 2020. Inflammatory responses of urban air PM modulated by chemical composition and different air quality situations in Nanjing, China. Environmental Research 192, 110382. https://doi.org/10.1016/j.envres.2020.110382.

Saarikoski, S., Niemi, J.V., Aurela, M., Pirjola, L., Kousa, A., Rönkkö, T., Timonen, H., 2021. Sources of black carbon at residential and traffic environments obtained by two source apportionment methods. Atmos. Chem. Phys. 21, 14851–14869. https://doi.org/10.5194/acp-21-14851-2021.

Sager, T.M., Castranova, V., 2009. Surface area of particle administered versus mass in determining the pulmonary toxicity of ultrafine and fine carbon black: comparison to ultrafine titanium dioxide. Part Fibre Toxicol. 6, 15. https://doi.org/10.1186/1743-8977-6-15.

Saha, P.K., Khlystov, A., Grieshop, A.P., 2015. Determining aerosol volatility parameters using a "dual thermodenuder" system: application to laboratory-generated organic aerosols. Aerosol Sci. Technol. 49, 620–632. https://doi.org/10.1080/02786826.2015.1056769.

Sand, M., Berntsen, T., von Salzen, K., et al., 2016. Response of Arctic temperature to changes in emissions of short-lived climate forcers. Nature Clim Change 6, 286–289. https://doi.org/10.1038/nclimate2880.

Schins, R.P.F., Knaapen, A.M., 2007. Genotoxicity of poorly soluble particles. Inhal. Toxicol. 19 (sup1), 189–198. https://doi.org/10.1080/08958370701496202.

Schmid, O., Stoeger, T., 2016. Surface area is the biologically most effective dose metric for acute nanoparticle toxicity in the lung. J. Aerosol Sci. 99, 133–143. https://doi.org/10.1016/j.jaerosci.2015.12.006.

Stanek, L.W., Sacks, J.D., Dutton, S.J., Dubois, J.J.B., 2011. Attributing health effects to apportioned components and sources of particulate matter: an evaluation of collective results. Atmos. Environ. 45 (32), 5655–5663. https://doi.org/10.1016/j.atmosenv.2011.07.023.

Sunjog, K., Kolarević, S., Héberger, K., Gačić, Z., Knežević-Vukčević, J., Vuković-Gačić, B., Lenhardt, M., 2013 Mayy. Comparison of comet assay parameters for estimation of genotoxicity by sum of ranking differences. Anal. Bioanal. Chem. 405 (14), 4879–4885. https://doi.org/10.1007/s00216-013-6909-y.

Timonen, H., Karjalainen, P., Saukko, E., Saarikoski, S., Aakko-Saksa, P., Simonen, P., Murtonen, T., Dal Maso, M., Kuuluvainen, H., Bloss, M., Ahlberg, E., Svenningsson, B., Pagels, J., Brune, W.H., Keskinen, J., Worsnop, D.R., Hillamo, R., Rönkkö, T., 2017. Influence of fuel ethanol content on primary emissions and secondary aerosol formation potential for a modern flex-fuel gasoline vehicle. Atmos. Chem. Phys. 17, 5311–5329. https://doi.org/10.5194/acp-17-5311-2017.

Timonen, H., Karjalainen, P., Aalto, P., Saarikoski, S., Mylläri, F., Karvosenoja, N., Jalava, P., Asmi, E., Aakko-Saksa, P., Saukkonen, N., Laine, T., Saarnio, K., Niemelä, N., Enroth, J., Väkevä, M., Oyola, P., Pagels, J., Ntziachristos, L., Cordero, R., Kuittinen, N., Niemi, J., Rönkkö, T., 2019. Adaptation of black carbon footprint concept would accelerate mitigation of global warming. Environ. Sci. Technol. 53 (21), 12153–12155. https://doi.org/10.1021/acs.est.9b05586.

Vodička, P., Schwarz, J., Brus, D., Ždímal, V., 2020. Online measurements of very low elemental and organic carbon concentrations in aerosols at a subarctic remote station. Atmospheric Environment (ISSN: 1352-2310) 226, 117380. https://doi.org/10.1016/j.atmosenv.2020.117380.

Wang, S.C., Flagan, R.C., 1990. Scanning electrical mobility spectrometer. Aerosol Sci. Technol. 13 (2), 230–240. https://doi.org/10.1080/02786829008959441.

Wang, J., Liu, D., Ge, X., Wu, Y., Shen, F., Chen, M., Zhao, J., Xie, C., Wang, Q., Xu, W., Zhang, J., Hu, J., Allan, J., Joshi, R., Fu, P., Coe, H., Sun, Y., 2019. Characterization of black carbon-containing fine particles in Beijing during wintertime. Atmos. Chem. Phys. 19, 447–458. https://doi.org/10.5194/acp-19-447-2019.

Wihersaari, H., Pirjola, L., Karjalainen, P., Saukko, E., Kuuluvainen, H., Kulmala, K., Keskinen, J., Rönkkö, T., 2020. Particulate emissions of a modern diesel passenger car under laboratory and real-world transient driving conditions. Environmental Pollution 265, 114948. https://doi.org/10.1016/j.envpol.2020.114948.

Xiao, T., Ling, T.M., Xu, H., Luo, F., Xue, J., Chen, C., Bai, J., Zhang, Q., Wang, Y., Bian, Q., Liu, Q., 2019. NF-κB-regulation of miR-155, via SOCS1/STAT3, is involved in the PM2.5-accelerated cell cycle and proliferation of human bronchial epithelial cells. Toxicology and Applied Pharmacology (ISSN: 0041-008X) 377, 114616. https://doi.org/10.1016/j.taap.2019.114616.

Yang, J., Huo, T., Zhang, X., et al., 2018. Oxidative stress and cell cycle arrest induced by short-term exposure to dustfall PM2.5 in A549 cells. Environ. Sci. Pollut. Res. 25, 22408–22419. https://doi.org/10.1007/s11356-017-0430-3.

Yang, Jun, Sakhvidi, Mohammad Javad Zare, de Hoogh, Kees, Vienneau, Danielle, Siemiatyck, Jack, Zins, Marie, Goldberg, Marcel, Chen, Jie, Lequy, Emeline, Jacquemin, Bénédicte, 2021. Long-term exposure to black carbon and mortality: A 28-year follow-up of the GAZEL cohort. Environment International (ISSN: 0160-4120) 157, 106805. https://doi.org/10.1016/j.envint.2021.106805.

Zhang, S., Chen, H., Wang, A., Liu, Y., Hou, H., Hu, Q., 2019. Genotoxicity evaluation of carbon monoxide and 1,3-butadiene using a new joint technology: the in vitro γH2AX HCS assay combined with air–liquid interface system. Toxicol. Mech. Methods 29 (1), 1–7. https://doi.org/10.1080/15376516.2018.1477897.